Soft Matter

PAPER

View Article Online
View Journal | View Issue

Cite this: *Soft Matter*, 2015, 11, 4315

Nonlinear elasticity and cavitation of a triblock copolymer gel†

Seyed Meysam Hashemnejad and Santanu Kundu*

Received 8th February 2015,
Accepted 19th April 2015

DOI: 10.1039/c5sm00330j

www.rsc.org/softmatter

Polymer gels are subjected to large-strain deformation during their applications. The gel deformation at large-strain is non-linear and can often lead to failure of the material. Here, we report the large-strain deformation behavior of a physically cross-linked, swollen triblock copolymer gel, which displays unique strain-stiffening response at large-strain. Investigations were performed using large amplitude oscillatory shear (LAOS) and custom developed cavitation rheology techniques. The Gent constitutive equation, which considers finite extensibility of midblock, was fitted with the LAOS data, thereby, linking the estimated parameters from LAOS analysis to the structure of the gel. The pressure responses obtained from the cavitation experiments were modeled using neo-Hookean and Gent constitutive equations. Our results capture the failure behavior of a gel with finite chain extensibility, initiated from a defect within the gel.

Introduction

Gels are a chemically or physically cross-linked polymer network swollen with a large amount of solvents. Despite a large amount of solvent content, gels behave like solid and the mechanical properties of gels can be tuned to match that of human tissues.[1–5] In addition, selecting polymers with an appropriate chemical structure, gels can be made responsive to external stimuli such as temperature, pH, electrical field, and light.[1,2,4–10] All these interesting properties make gels to be useful in many potential applications including tissue engineering, drug delivery vehicles, superabsorbents, gel-based sensors, soft robots/machines, *etc.*[1,2,4,11–16] An understanding of gel mechanical properties is essential, particularly, if the gel is expected to be mechanically deformed during its applications. The mechanical properties of a gel depend on the polymer volume fraction; degree, nature and strength of crosslinking; polymer chain architecture; time and length scales involved with the diffusion of small solvent molecules in and out of the network structure.[4,5,7,14] At low-strain, the polymer chains do not deviate significantly from the equilibrium conformation, as a result, the modulus almost remains constant. However, with increasing applied-strain, the polymer chains are deformed from their equilibrium conformation, often followed by chain-scissions or dissociation of physical bonds, leading to failure of the material. During the large-strain deformation process, the elastic modulus of a gel can decrease (strain-soften) or increase (strain-stiffen) before fracture takes place.[4,17–20] Finite-extensibility of polymer chains has been attributed to the strain-stiffening behavior at large-strain, whereas, slippage at the entanglement points, defects present in the free-radical polymerized network, can result in strain-softening behavior.[17,19,21] However, our understanding of the failure mechanism of gels at large-strain is incomplete.

At low-strain, in the linear viscoelastic region, gel mechanical properties can be determined by conventional rheological experiments, such as small amplitude oscillatory shear.[22] In comparison, characterizing mechanical properties of a gel or any soft-materials at large-strain is challenging. This is attributed to the soft and slippery nature of gels, for which performing conventional mechanical tests such as tensile tests is difficult. As a result, large-strain deformation behavior of swollen gels is not well understood and several theoretical framework and experimental methodologies are being developed to overcome this challenge.[23–31] The compression technique, in which a cylindrical sample is compressed at different strain rates, is one of the most widely used techniques to investigate the gel mechanical properties.[30,31] This method provides interesting insight into the gel mechanical properties.[30,31] However, in these experiments the samples need to be prepared with specific dimensions, which can be difficult to obtain for very soft gels.

LAOS (large amplitude oscillatory shear) experiments are increasingly being used to evaluate the large-strain (in the non-linear viscoelastic region) behavior of soft materials.[32,33] Fourier transformation (FT) of raw stress–strain data provides a number

Dave C. Swalm School of Chemical Engineering, Mississippi State University, MS State, MS, USA. E-mail: santanukundu@che.msstate.edu

† Electronic supplementary information (ESI) available: Gelation temperature (ESI 1), the effect of geometry on shear-rheology (ESI 2), moduli as a function of frequency (ESI 3), initiation and propagation of fracture in a gel during LAOS (ESI 4), the effect of polymer volume fractions on the shear modulus (ESI 5), and the ratio of elastic moduli from cavitation and shear experiments (ESI 6). See DOI: 10.1039/c5sm00330j

of parameters describing the viscoelastic response of a material in the nonlinear region.[34] Ewoldt *et al.*[35] utilized the geometric interpretation of stress–strain data proposed by Cho *et al.*[36] and applied orthogonal Chebyshev polynomial of the first kind for describing stress–strain responses. Here, we apply this framework to investigate the gel mechanical properties at large-strain, therefore, linking the mathematical parameters estimated from LAOS analysis to the gel structure.

Cavitation rheology is another measurement technique to investigate the large-strain deformation behavior of polymer gels at different length scales and at any arbitrary locations within a gel.[37] This technique involves inserting a syringe–needle within a gel and pressurizing a fluid (*e.g.* air, water) inside the syringe–needle to deform the gel at the tip of the needle. Beyond a critical pressure, the gel either cavitates or fractures and the critical pressure is related to the elasticity of the soft material and the surface energy of the media and the gel interface. Varying the needle radius allows us to investigate the deformation behavior of soft materials as a function of length scale ($\sim$10 μm to 1000 μm). Cavitation rheology has been adapted to various polymer gels and biological networks.[38–40] However, determining the true relationship between the critical pressure, the mechanism of cavity growth inside an elastomer or a gel, and the local elastic modulus is a complex problem,[40–45] particularly for a strain-stiffening gel, as explained here. We also attempt to model the gel cavitation phenomena using the Gent model, in comparison to neo-Hookean models used in earlier studies.[40–48]

Here, we investigate the large-strain deformation behavior of a physically associating, thermoreversible, model gel using both LAOS and cavitation rheology. This model gel consists of a triblock copolymer, poly methylmethacrylate–poly *n*-butylacrylate–poly methylmethacrylate (PMMA–PnBA–PMMA), dissolved in a midblock selective solvent.[20,49] Cavitation rheology measurements as a function of temperature have been conducted. LAOS experiments capture the strain-stiffening responses of the model gel. The estimated parameters from LAOS data describing the strain-stiffening responses are linked to the Gent constitutive model, which considers finite chain extensibility and the resulting strain-stiffening behavior. We applied such understanding to explain the experimental observations from cavitation rheology. Our results capture the failure behavior of triblock copolymer gels with finite chain extensibility, initiated from a defect within the gel. In addition, strain-stiffening response of our gel is similar to that observed in biological tissues and our results will also be relevant to the cavitation phenomena observed in biological tissues.[50]

Experimental section

Materials

A triblock copolymer, PMMA–PnBA–PMMA, with an end-block (PMMA) molecular weight of 9000 g mol^{-1} and a mid-block (PnBA) molecular weight of 53 000 g mol^{-1}, was kindly provided by Kuraray Corporation. Gels with different polymer concentrations (5, 7 and 10% v/v) were prepared by dissolving a polymer of appropriate quantity at 70 °C in 2-ethyl-1-hexanol (Fisher Scientific), a midblock selective solvent.

Rheological experiments

Rheological measurements were conducted using a TA instrument HR-2 rheometer. Most of the experiments were performed using a 25 mm cone-plate geometry. Also, 25 mm parallel-plate geometry was used to visualize the fracture of the gel at large-strain. Results from both cone-plate and parallel-plate geometries did not show a significant difference in responses. The rheometer is fitted with a Peltier system. The samples were loaded in the rheometer in the liquid state (at 50 °C) and were then cooled to obtain gels.

Cavitation experiments

Cavitation experiments were performed using a custom-built set-up at 22 °C (room temperature) and at 6 °C. An ice bath was used to maintain the temperature at 6 °C. In cavitation experiments, a syringe–needle was inserted into a gel at an arbitrary location. The syringe–needle was connected to a syringe and the air within the system (confined by the syringe plunger and the gel at the tip of the needle) was pressurized using a syringe pump (New Era). A pressure transducer (Px26 series from Omega Engineering) was used to record the system pressure as a function of time. Images of gel deformation at the tip of the needle were captured using a digital camera (Basler). A custom written program in LabVIEW was used to control the experiments and to collect data and images.

Results and Discussion

PMMA–PnBA–PMMA gel

A thermoreversible, physically associating model gel, studied in detail by Shull and coworkers,[20,28,49,51,52] is considered in this study. Here, a PMMA–PnBA–PMMA triblock copolymer is dissolved in a midblock selective solvent, 2-ethyl-1-hexanol. At high temperature the polymer is completely soluble in the solvent, but as the temperature is reduced, solubility of the PMMA end-blocks in the solvent decreases. Subsequently, the end-blocks of multiple polymer chains self-assemble into aggregates or micelles and these aggregates are connected by the soluble PnBA midblock chains. As a result, a three dimensional network structure is obtained, where the PMMA aggregates act as the physical crosslinking points.

Transition from the liquid to gel like structure with a decrease of temperature was monitored using rheological experiments (Fig. S1, ESI†).[20,49] At the transition temperature, defined as the critical micelle temperature or cmt,[20,49] the elastic modulus is equal to the viscous modulus and below the cmt the elastic modulus is higher than the viscous modulus, *i.e.*, the sample behaves like a soft solid. Near the cmt, the aggregates are still swollen with some amount of solvents and the relaxation process involving exchange of endblocks in and out of the aggregates is fast. With a further decrease of temperature, solubility of the endblocks in the solvent decreases and the solvent is expelled from the aggregates. During this process, the aggregates reach a

glassy state, correspondingly, a glass transition temperature (T_g) is observed.[20,49] Below T_g, the relaxation process slows down significantly.[49,52] The long relaxation time leads to stretching of midblock to its fully-stretched length before being pulled-out of the aggregates and the resulting strain-stiffening behavior of this gel as a result of mechanical deformation. For the triblock gel considered here, T_g is higher than the room temperature[20] and the sample behaves like a gel at the experimental temperatures of 22 °C and 6 °C. The gelation process is thermoreversible in nature, *i.e.*, the gel sample can be heated to liquid form and the deformation history can be erased. It is beneficial, as a single sample can be tested multiple times without any previous deformation history and the experimental uncertainties caused from sample to sample variations can be minimized.

Large amplitude oscillatory shear (LAOS)

Dynamic oscillatory shear experiments are performed to investigate the bulk rheological properties of soft materials and the parameters of interests are elastic (storage) and viscous (loss) moduli. The shear stress response of a viscoelastic material subjected to a shear strain, $\gamma = \gamma_0 \sin(\omega t)$, can be written as:[32]

$$\tau(t) = \sum_{n:\text{odd}} \tau_n \sin(n\omega t + \delta_n) \quad (1)$$

where, γ_0 is the strain amplitude, ω is the angular frequency, τ_n and δ_n are the nth harmonic stress amplitude and phase angle, respectively. By using trigonometric identities it can be decomposed into a summation of elastic and viscous contribution:

$$\tau(t) = \gamma_0 \sum_{n:\text{odd}} \left(G_n^{'}(\omega, \gamma_0) \sin n\omega t + G_n^{''}(\omega, \gamma_0) \cos n\omega t \right) \quad (2)$$

where $G_n^{'}$ and $G_n^{''}$ are viscoelastic moduli. In the linear viscoelastic region, the first harmonic of eqn (2) is enough to capture the elastic and viscous behavior of a gel, *i.e.*, $G_1^{''} = G_n^{''}$ (storage modulus: elastic contribution) and $G_1^{''} = G_n^{''}$ (loss modulus: viscous contribution). Plotting stress *vs.* strain data (Lissajous–Bowditch curves) in the linear regime yields an ellipse. At larger strain, the Lissajous–Bowditch curves are not perfectly elliptical but distorted in nature and the stress response cannot be captured by using a single harmonic and higher order terms of the eqn (2) are needed. Thus, G' and G'' do not uniquely describe the storage and loss moduli.

The stress responses can also be decomposed using Chebyshev polynomials of the first kind as the orthogonal basis functions:[35]

$$\tau(t) = \gamma_0 \sum_{n:\text{odd}} e_n T_n(x) + \dot{\gamma}_0 \sum_{n:\text{odd}} v_n T_n(y) \quad (3)$$

where $T_n(x)$ and $T_n(y)$ are the nth order Chebyshev polynomials of the first kind, $\dot{\gamma}_0$ is the strain rate amplitude, $x = \gamma/\gamma_0$, $y = \dot{\gamma}/\dot{\gamma}_0$, and e_n and v_n are the elastic and viscous Chebyshev coefficients, respectively. In the linear viscoelastic region, eqn (3) reduces to $\tau(t) = \gamma_0 e_1 T_1(x) + \dot{\gamma}_0 v_1 T_1(y) = \gamma_0 e_1 x + \dot{\gamma}_0 v_1 y$, which is related to eqn (2) as $e_1 = G_1^{'} = G^{'}$ and $\nu_1 = G_1^{''}/\omega = G^{''}/\omega$. In the non-linear regime, the higher order coefficients are not zero. The sign and magnitude of the third order Chebyshev coefficients represent the strain-stiffening ($e_3 > 0$) or strain-softening ($e_3 < 0$) and shear-thickening ($v_3 > 0$) or shear-thinning ($v_3 < 0$) behavior of a material.

Using the framework discussed above the rheological responses of the triblock gel samples were analyzed. The results from LAOS experiments, performed using a 25 mm cone-plate geometry (the results are independent of geometry; Fig. S2, ESI†) at 22 °C and at a frequency (ω) of 1 rad s^{-1}, are shown in Fig. 1a and b. Fig. 1a displayed the storage modulus, $G_1^{'}$, and the loss modulus, $G_1^{''}$, estimated by the rheometer software. Both in linear and nonlinear regions, these values were obtained by considering the first harmonic only. $G_1^{'}$ values are much higher than $G_1^{''}$, confirming the gel (soft-solid) like behavior of our system. Also, at large-strain, $G_1^{'}$ values increase with the increase of strain, indicating the strain-stiffening nature of this gel. The corresponding stress–strain curves (Lissajous–Bowditch curves) are shown in Fig. 1b. The results clearly reveal the transition from linear to non-linear responses, as the elliptical stress–strain responses become distorted with increasing strain amplitude. Strain amplitude $\gamma_0 < 39\%$, represents the linear viscoelastic region (up to the point 13 in Fig. 1b). For larger strain values, a transition from linear to non-linear responses takes place and higher harmonics are required to capture the stress responses, as $G_1^{'}$ underestimates the elastic modulus values. Therefore, we estimated the third-order Chebyshev coefficients, e_3, using MITlaos software. As shown in Fig. 1c, e_3 have positive values in the non-linear region, confirming the strain-stiffening response of the gel.

The effects of frequency on storage and loss moduli in both linear and non-linear viscoelastic regions are also investigated (Fig. S3, ESI†). Similar to strain-sweep tests, $G_1^{'}$ values are found to be much higher than that of $G_1^{''}$. Also, $G_1^{'}$ increases slightly with the increasing frequency. Both these observations are typical to gel like materials.[53] Frequency dependency of moduli decreases as the temperature was decreased from 22 °C to 6 °C. The reduction of temperature results in an increase of relaxation time and the gel behaves more elastically.

Changes in stress–strain responses with increasing frequency and strain amplitude provide us some interesting insights. Fig. 2 displays stress–strain responses over a frequency (ω) range of 1 rad s^{-1} to 30 rad s^{-1} (higher frequency data not considered due to the inertia effect of a stress-controlled rheometer) and a strain amplitude (γ_0) range of 10% to 200%. Each curve is provided with the corresponding e_3 and $G_1^{'}$ values. In the linear viscoelastic region, for $\gamma_0 = 10\%$, e_3 is equal to zero up to a frequency of 10 rad s^{-1}, and a small positive value is observed at higher frequencies. At a higher strain value, such as $\gamma_0 = 200\%$, a significant increase of e_3 (as high as 3 times) is observed with increasing frequency, *i.e.*, the strain-stiffening response enhances with increasing frequency. At high frequencies there will not be enough time for the exchange of PMMA end blocks in and out of the aggregates and the enhancement of strain-stiffening takes place.

Gent model. For elastic materials, strain energy functions (W) relate the extension ratio (λ) to elastic energy.[22,42,54] The strain energy function for the Gent model, considering finite

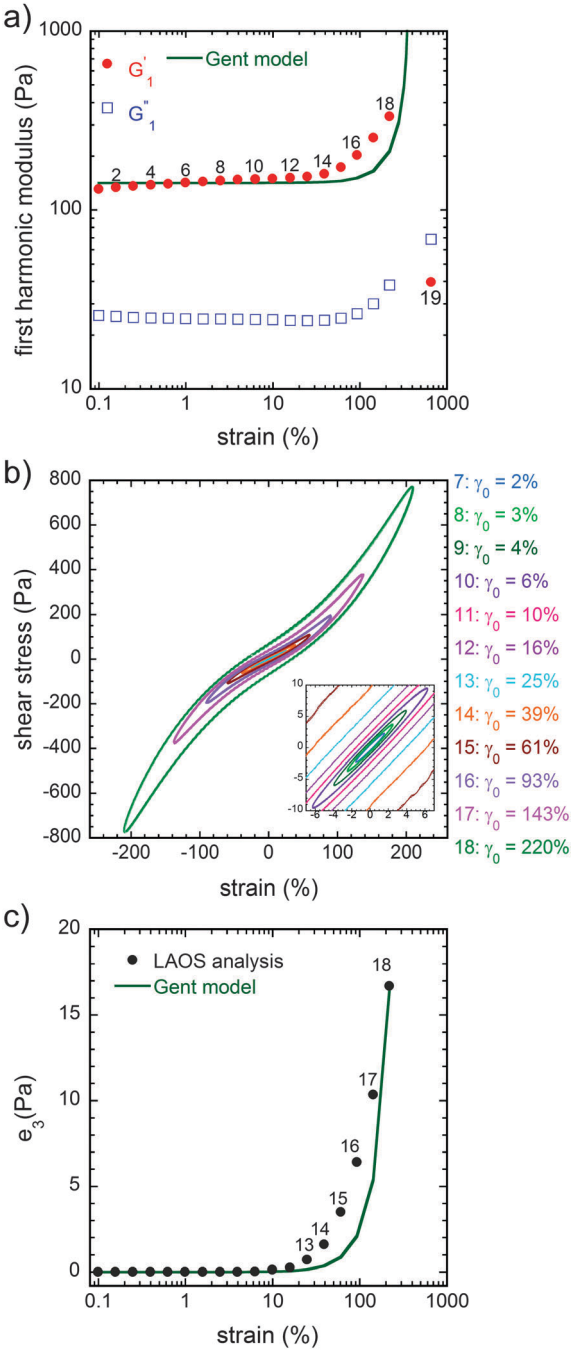

Fig. 1 Linear and non-linear viscoelastic responses of a PMMA–PnBA–PMMA triblock copolymer gel with a polymer volume fraction (ϕ) of 0.05. Experiments were performed at 22 °C and at a frequency (ω) of 1 rad s^{-1}. (a) The closed and open symbols are storage (G_1') and loss (G_1'') moduli estimated by the rheometer software. The solid line is e_1, predicted from the Gent model (eqn (7)) considering a maximum stretch ratio (λ_m) of 380%. (b) Lissajous–Bowditch curves as a function of strain. (c) Closed symbols are the third Chebyshev coefficients (e_3) estimated form experimental data and the solid line is the prediction of the Gent model (eqn (8)).

chain-extensibility, is:[55]

$$W = -\frac{EJ_m}{6}\ln\left(1-\frac{J_1}{J_m}\right) = -\frac{G_{lin}J_m}{2}\ln\left(1-\frac{J_1}{J_m}\right) \quad (4)$$

where, E is Young's modulus, $J_1 = \lambda_1^2 + \lambda_2^2 + \lambda_3^2 - 3$ (λ_is are the extension ratios in the principal stretch directions), J_m corresponds to the maximum extensibility or maximum chain extension, λ_m; G_{lin} is the linear elastic modulus and is equal to $E/3$ for Poisson's ratio = 0.5. The Gent model approaches to the neo-Hookean model when maximum chain extensibility approaches infinity, *i.e.*, $\lambda_m \to \infty, J_m \to \infty$.[54]

As observed in rheological results, the elastic modulus of our gel is much higher than the viscous modulus. Therefore, for our analysis we assumed that viscous dissipation is negligible and the elastic stress is approximately equal to the total stress ($\tau_{elastic} \approx \tau$). The shear stress as a function of strain can be written as:[35]

$$\tau = \gamma f(\gamma) \quad (5)$$

where γ is the shear strain and $f(\gamma)$ is the shear modulus as a function of γ. At small strain, $f(\gamma)$ approaches a constant modulus (G_{lin}). For simple-shear experiments, shear strain is related to the extension ratio as $\gamma = \lambda - 1/\lambda$. Also, shear stress is the derivative of the strain energy function with respect to strain.[54] Thus, from strain the energy function for the Gent model (eqn (4)) we have:

$$f(\gamma) = \frac{G_{lin}}{1-\left(\frac{\gamma^2}{J_m}\right)} = \frac{G_{lin}}{1-\left(\frac{\gamma}{\gamma_m}\right)^2} \quad (6)$$

It has been shown that[35] $\left.\frac{d\tau}{d\gamma}\right|_{\gamma=0} = e_1 - 3e_3 + \ldots$, $\left.\frac{\tau}{\gamma}\right|_{\gamma=\pm\gamma_0} = e_1 + e_3 + \ldots$ Using these relationships, the first and third-order Chebyshev coefficients, e_1 and e_3, can be provided for the Gent model as:

$$e_1 = \frac{1}{4}G_{lin} + \frac{3}{4}G_{lin}\frac{1}{1-\left(\frac{\gamma}{\gamma_m}\right)^2} \quad (7)$$

$$e_3 = \frac{1}{4}G_{lin}\frac{\left(\frac{\gamma}{\gamma_m}\right)^2}{1-\left(\frac{\gamma}{\gamma_m}\right)^2} \quad (8)$$

The third-order Chebyshev coefficient for the Gent model is always a positive number ($\gamma/\gamma_m < 1$), predicting a strain stiffening behavior. The summation of e_1 and e_3 is equal to $f(\gamma)$ in eqn (6).

The maximum extension ratio for the gel with a polymer volume fraction (ϕ) of 0.05 was estimated based on the small angle X-ray scattering (SAXS) data reported in the literature.[20,51] During shearing or any mechanical deformation, the PnBA chains connecting the PMMA aggregates are stretched and the fully stretched length of the PnBA chains (molecular weight 53 000 g mol^{-1}) is estimated to be $\approx$105 nm and the unstretched length estimated from SAXS data is $\approx$28 nm.[20] This results in maximum extensibility, $\lambda_m \approx 3.8$. This value is considered for our analysis here.

The Gent model (eqn (7) and (8)) was fitted to the experimental data (Fig. 1a and c) and the model captures the experimental data

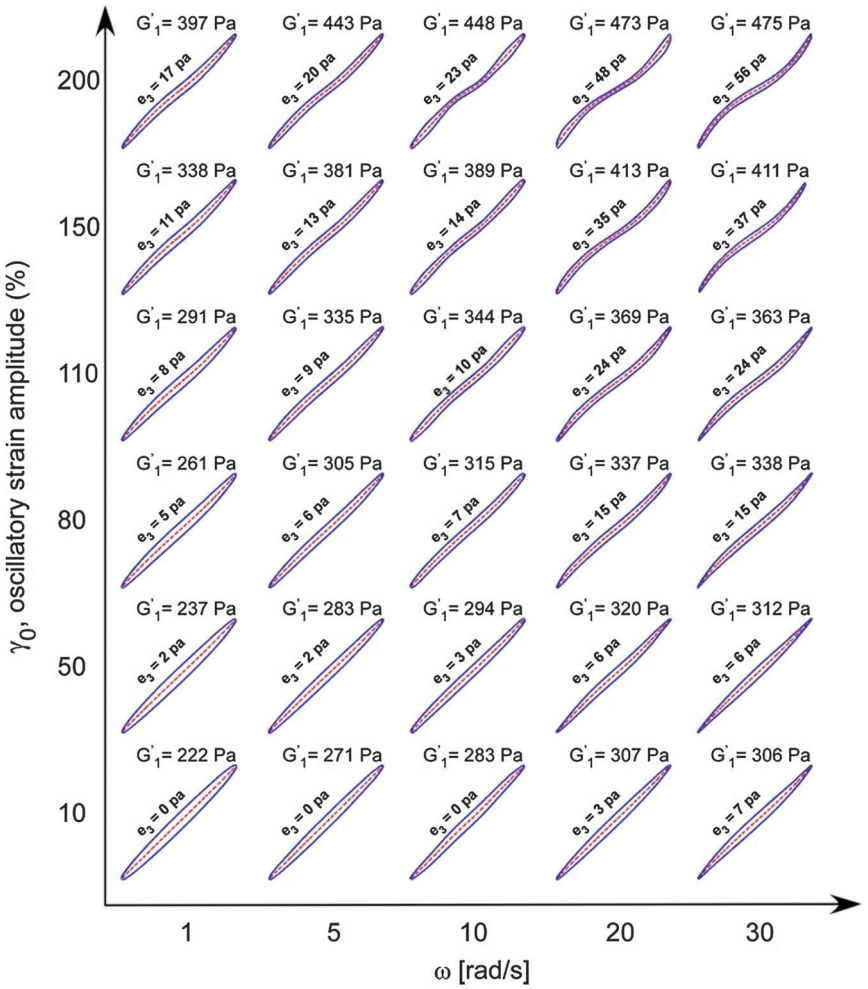

Fig. 2 Lissajous–Bowditch curves as a function of frequency and strain amplitude. Red dashed lines represent the pure elastic stress responses of the gel. e_3, and $G_1^{'}$ values are indicated for each oscillatory test. Here, the polymer volume fraction (ϕ) is 0.05 and experiments were conducted at 22 °C.

reasonably well. There is a similar trend in the prediction of the elastic modulus ($G_1^{'}$ or e_1) and e_3, as both increase rapidly at large-strain. Using the Gent model in the LAOS formulation, we were able to elucidate the physical significance of the mathematical coefficients estimated from the analysis. The coefficient, e_3 only represents the non-linear response of the gel, whereas, e_1 has contributions from both linear and non-linear components.

During rheological experiments, a fracture in the gel sample was observed at a strain value of $\sim$350%, as a result, a drop in the modulus value was observed (point 19 on Fig. 1a). Fracture of this gel during shear has been related to the strain-localization or non-homogeneous strain field[28] and the preliminary observation indicates that fracture initiates in the bulk (Fig. S4, ESI†). However, it is interesting to note that the strain value for fracture is very close to the maximum strain value that can be achieved considering finite chain extensibility.

Cavitation

Cavitation phenomena are observed in elastomeric networks[42] and even in human brain subjected to shock wave.[50] Cavitation is caused by elastic instability. It is considered to be a reversible process and no fracture is involved.[43] Utilizing cavitation phenomena, a measurement technique (cavitation rheology) has been developed for investigating local mechanical properties of soft solids.[38,40,43–45] Although the experimental observation of cavity formation at a critical pressures is similar for all gels, the main challenge in cavitation rheology is determining the mathematical relationship that relates the cavitation pressure to the mechanical properties. The relationship depends on the strain energy function used. Now, the strain energy function must be physically meaningful and should capture the rheological responses adequately. The previous section shows that the Gent model can be fitted with the experimental data reasonably well. It captures the strain-stiffening behavior of the PMMA–PnBA–PMMA gel considered here and also verifies our assumption that the maximum extensibility of this gel is $\approx$3.8. The rheological results are also used to explain the experimental observations from the cavitation rheology experiments. Here, experiments were performed for gels with different polymer volume fractions, at different pumping/compression rates, and at a temperature different than room temperature.

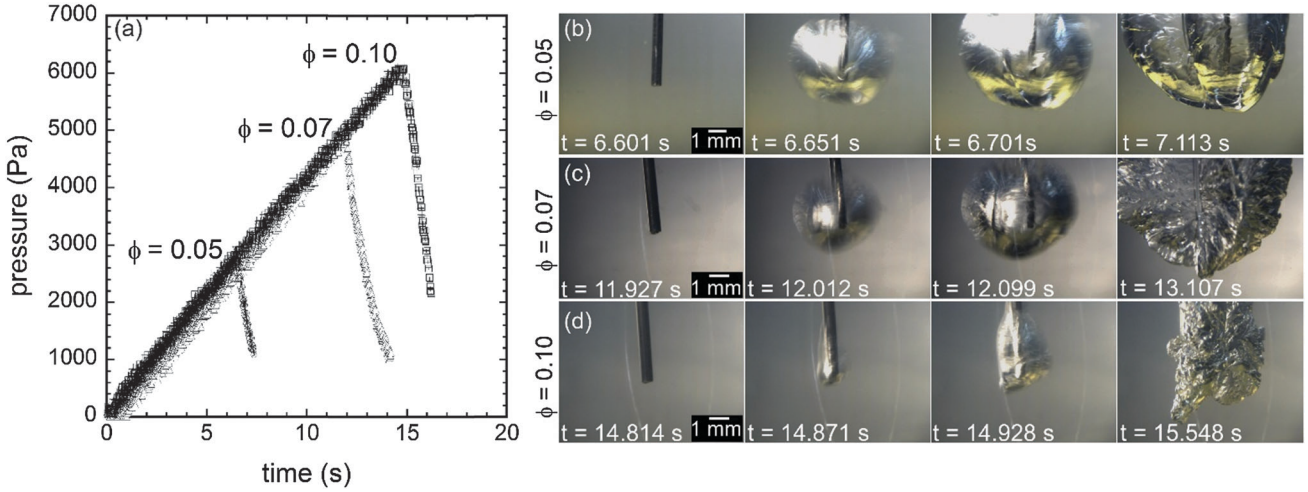

Fig. 3 (a) Pressure as a function of time for three polymer volume fractions, ϕ = 0.05, 0.07, and 0.10. (b–d) Micrographs of cavity growth at and after the critical pressure for (b) ϕ = 0.05, (c) ϕ = 0.07, (d) ϕ = 0.10. Needle radius, r_{in} = 156 μm. Experimental temperature 22 °C.

Effects of polymer volume fractions. Fig. 3a displays the pressure responses during cavitation experiments for polymer volume fractions (ϕ) of 0.05, 0.07, and 0.10. For all these gels the system pressure increases linearly with time during pressurization to a maximum value (defined as critical pressure, P_c) before a sudden drop of pressure takes place. Fig. 3b–d display the deformation of these gels at the tip of the needle, captured at and after P_c. The micrographs indicate that at P_c a cavity forms rapidly at the tip of the needle inside the gel. The sudden formation of cavity results in a decrease of pressure. The critical pressure increases with the increase of polymer volume fractions. This is expected as critical pressure scales with the elastic modulus of a material and with the increase of polymer concentration, the elastic modulus of a gel increases (Fig. S5, ESI†).

Although cavity formation was observed at P_c for all of the volume fractions investigated here, the nature of cavity growth depends on the polymer volume fraction. For ϕ = 0.05, the cavity maintained its spherical shape, whereas, for ϕ = 0.10 the cavity transitioned to asymmetric fracture like response. Considering the expansion ratio defined as $\lambda = (A_c/A_{c0})^{1/2}$, where, A_c is the surface area of the cavity at any instance and A_{c0} is the inner cross-sectional area of the needle (the initial area), we have observed λ of as high as 15. As discussed earlier, the maximum possible stretch ratio for the PnBA chains is $\approx$3.8. Therefore, during cavity growth PnBA chains must have been pulled out of the PMMA aggregates.

Effects of the compression/pumping rate. Mechanical response of a viscoelastic material depends on the applied strain-rate or the time-scale associated with mechanical deformation with respect to the relaxation time of the material. The frequency sweep data (Fig. 2) indicate that the non-linearity and the modulus of this gel depend on the applied frequency (related to the strain-rate). To investigate further, cavitation experiments were performed at different pumping/compression rates, which directly correspond to gel deformation at the needle-tip for different strain-rates. Fig. 4 displays results for a gel with ϕ = 0.05 in which pumping/compression rates were varied from 0.01 to 25 mL min^{-1}. Interestingly, critical pressure for a pumping rate of 0.01 mL min^{-1} is significantly lower than that observed for the pumping rate of 0.5 mL min^{-1}. At a low pumping rate the experimental time scale is comparable to the gel relaxation time, which is higher than 100 s.[52] As discussed below, cavitation phenomena observed here involve the chain pull-out of the aggregates and if the experimental time-scale is similar to the relaxation time, the pull-out process will be easier and as a result a decrease in P_c can be observed. With an increasing pressurization rate, a small increase of P_c was observed. However, to observe a significant change in P_c, as one might expect by looking at the frequency sweep data, it is

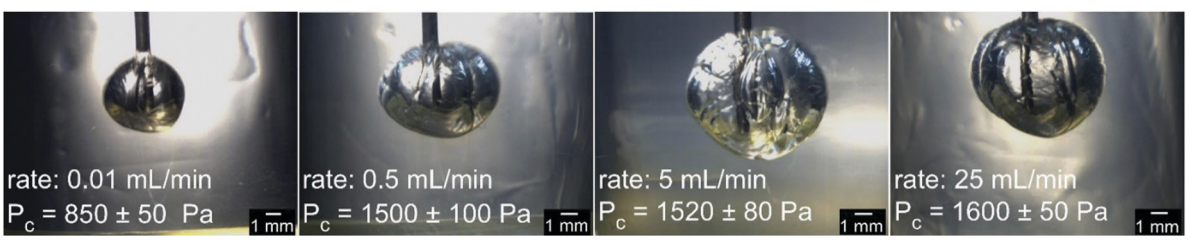

Fig. 4 Images are at critical pressure for different compression/pumping rates. Polymer volume fraction, ϕ = 0.05 and needle radius, r_{in} = 302 μm.

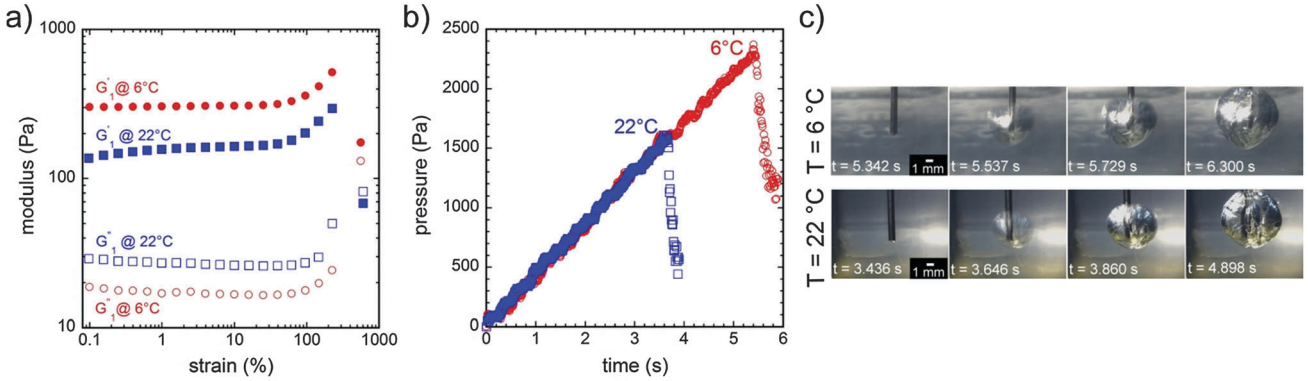

Fig. 5 (a) Moduli as a function of strain at 6 °C and 22 °C. (b) Temperature dependence on cavitation, and (c) initiation and growth of cavity. Here, polymer volume fraction ϕ = 0.05, and needle radius, r_{in} = 302 μm.

likely that the rate of pressurization needs to be increased significantly, however; such a high rate cannot be achieved in our present set-up.

Effects of temperature. To identify the temperature dependence on cavitation, we also conducted the cavitation experiments at ≈ 6 °C using an ice bath. Fig. 5 displays the results obtained from shear rheology and cavitation experiments for a gel with ϕ = 0.05 at 6 and 22 °C. As expected, the storage modulus increases with the decrease of temperature (Fig. 5a); a storage modulus of ≈ 160 Pa at 10% strain and at 22 °C increases to ≈310 Pa at 6 °C for the same strain value, *i.e.*, the storage modulus increased by two times. Interestingly, at both these temperatures, during shearing, fracture of the gel took place at a similar strain value. For cavitation experiments, a higher critical pressure was observed at 6 °C. As lowering temperature results in an increase of the shear-modulus, the increase of P_c in cavitation experiments is expected, however, P_c increases by approximately 1.5 times, lower than that observed in shear-rheology experiments. Initiation and growth of cavity at both these temperatures were found to be similar.

Model prediction for pressure responses. We have shown that the Gent model can capture the LAOS data reasonably well including the strain-stiffening behavior and the maximum chain extensibility. Here, we use the Gent model to explain the cavitation phenomena. We also consider the neo-Hookean model, which is used in earlier studies to describe cavitation.[37,43]

The pressure *vs.* time responses presented above can be described using the continuum mechanics approach. It is assumed that during pressurization a spherical cap forms at the tip of the needle. Consequently, pressure at any instance can be given by, $P = \Gamma\, dA/dV + \sigma$,[43] where Γ is the surface energy, σ is the mechanical stress near the tip that the gel experiences, A and V are the surface area and volume of the cap, respectively. The stress σ can be defined using various strain energy functions. For the Gent strain energy function:[42,43,55]

$$P_{\text{Gent}} = \frac{4\Gamma}{r_{in}}\left(\frac{(\lambda^2-1)^{\frac{1}{2}}}{\lambda^2}\right) + \frac{2E}{3}\int_1^{\lambda}\frac{\lambda^{-2}+\lambda^{-5}}{\left(1-\frac{J_1}{J_m}\right)}d\lambda \qquad (9)$$

here, λ is the expansion ratio defined as $\lambda = (A_c/A_{c0})^{1/2}$, where, A_c is the surface area of the cavity at any instance and A_{c0} is the inner cross-sectional area of the needle (the initial area). If $J_m \to \infty$, pressure for neo-Hookean solid is given by:[43]

$$P_{\text{neo-Hookean}} = \frac{4\Gamma}{r_{in}}\left(\frac{(\lambda^2-1)^{\frac{1}{2}}}{\lambda^2}\right) + E\left(\frac{5}{6}-\frac{2}{3\lambda}-\frac{1}{6\lambda^4}\right) \qquad (10)$$

These functions can be used to track the pressure response during the cavitation experiment as a function of time. Considering that the experimental set-up is a close system (the air volume confined by the syringe plunger and the gel at the tip of the needle), air is an ideal gas, and no diffusion of air into the gel takes place while pressurizing, we can write:

$$PV = P_0V_0 \qquad (11)$$

where, P_0 is the initial system pressure (atmospheric pressure), V_0 is the initial system volume. Similarly, P and V are the system pressure and volume, respectively, at time, t, during the cavitation experiment. The system volume at any instance t can be written as:[37]

$$V = V_0 - \mu t + V_c \qquad (12)$$

V_c is the cavity volume at the syringe–needle tip and μ is the pumping/compression rate. During the initial stage of compression, when V_c is much smaller than V_0, eqn (11) and (12) yield:

$$\frac{P_1}{P_0} = \frac{\mu}{V_0}t \qquad (13)$$

where, $P_1 = P - P_0$, the gauge pressure measured by the pressure transducer, as reported in Fig. 3a and 5b. The linear behavior of eqn (13) is evident in Fig. 3a and 5b. This allows us to determine the system volume from the initial slope of the P *vs.* time experimental data. For the results presented in Fig. 3a and 5b, $V_0 \approx$ 24 mL.

Now, assuming a spherical cap at the tip of needle, the cavity volume can be written as:

$$V_c = \frac{\pi {r_{in}}^3}{6}(\lambda^2+2)(\lambda^2-1)^{\frac{1}{2}} \qquad (14)$$

From eqn (10)–(12) and (14), for the neo-Hookean gel, we obtain:

$$P_0V_0 - \left[\frac{4\Gamma}{r_{in}}\left(\frac{(\lambda^2-1)^{\frac{1}{2}}}{\lambda^2}\right) + E\left(\frac{5}{6}-\frac{2}{3\lambda}-\frac{1}{6\lambda^4}\right)\right] \times \left[V_0 - \mu t + \left(\frac{\pi {r_{in}}^3}{6}(\lambda^2+2)(\lambda^2-1)^{\frac{1}{2}}\right)\right] = 0 \quad (15)$$

And for the Gent gel:

$$P_0V_0 - \left[\frac{4\Gamma}{r_{in}}\left(\frac{(\lambda^2-1)^{\frac{1}{2}}}{\lambda^2}\right) + \frac{2E}{3}\int_1^{\lambda}\frac{\lambda^{-2}+\lambda^{-5}}{[1-J_1/J_m]}d\lambda\right] \times \left[V_0 - \mu t + \left(\frac{\pi {r_{in}}^3}{6}(\lambda^2+2)(\lambda^2-1)^{\frac{1}{2}}\right)\right] = 0 \quad (16)$$

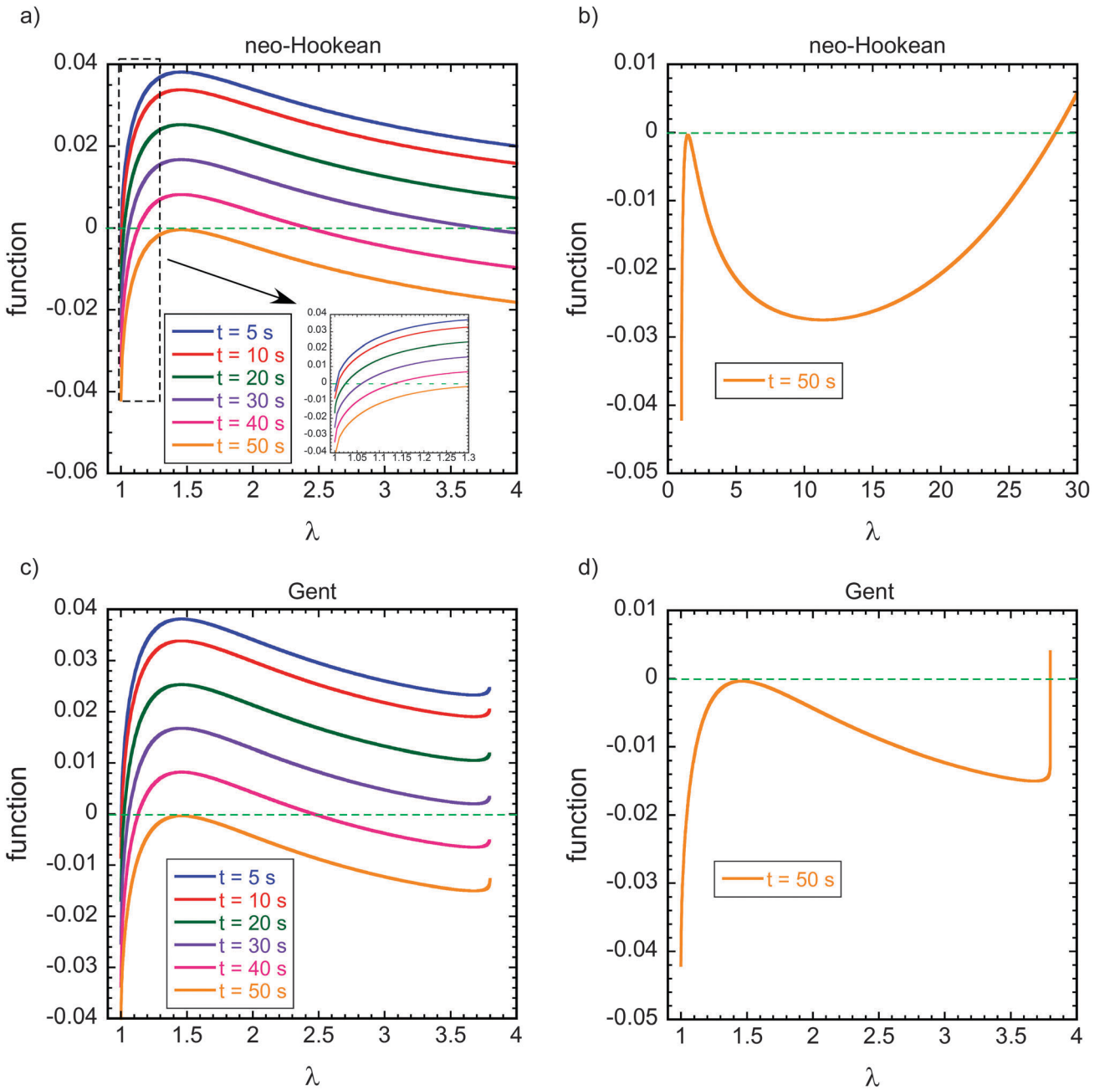

Fig. 6 Eqn (15) (neo-Hookean) model for different time steps before (a) and after instability point (b). Eqn (16) (Gent model with λ_m = 3.8) for different time steps before (c) and after instability point (d). Here, for model prediction, E = 300 Pa, r_{in} = 302 μm, P_0 = 101 325 Pa, V_0 = 24 mL, μ = 0.5 mL min^{-1}, Γ = 0.25 J m^{-2} are used.

Fig. 6 displays the above functions (the left side of eqn (15) and (16)) plotted as a function of λ for different time steps. The values of the elastic modulus (E), initial system volume (V_0) and pressure (P_0), pumping rate (μ), and surface energy (Γ) used here are listed in the caption of Fig. 6. Here surface energy (Γ) is a fitting parameter. The roots/solutions for these objective functions will be the values of λ for which these functions are equal to zero (eqn (15) and (16)). The objective function for the neo-Hookean model has a solution in between $1 < \lambda < 1.4$ for $t < 50$ s (Fig. 6a). However, for $t > 50$ s, the solution jumps to a very high number, $\lambda \approx 28$ (Fig. 6b). This jump is expected for the neo-Hookean model, as infinite extensibility is assumed. The objective function for the Gent model behaves similar to the neo-Hookean model, however, λ can only

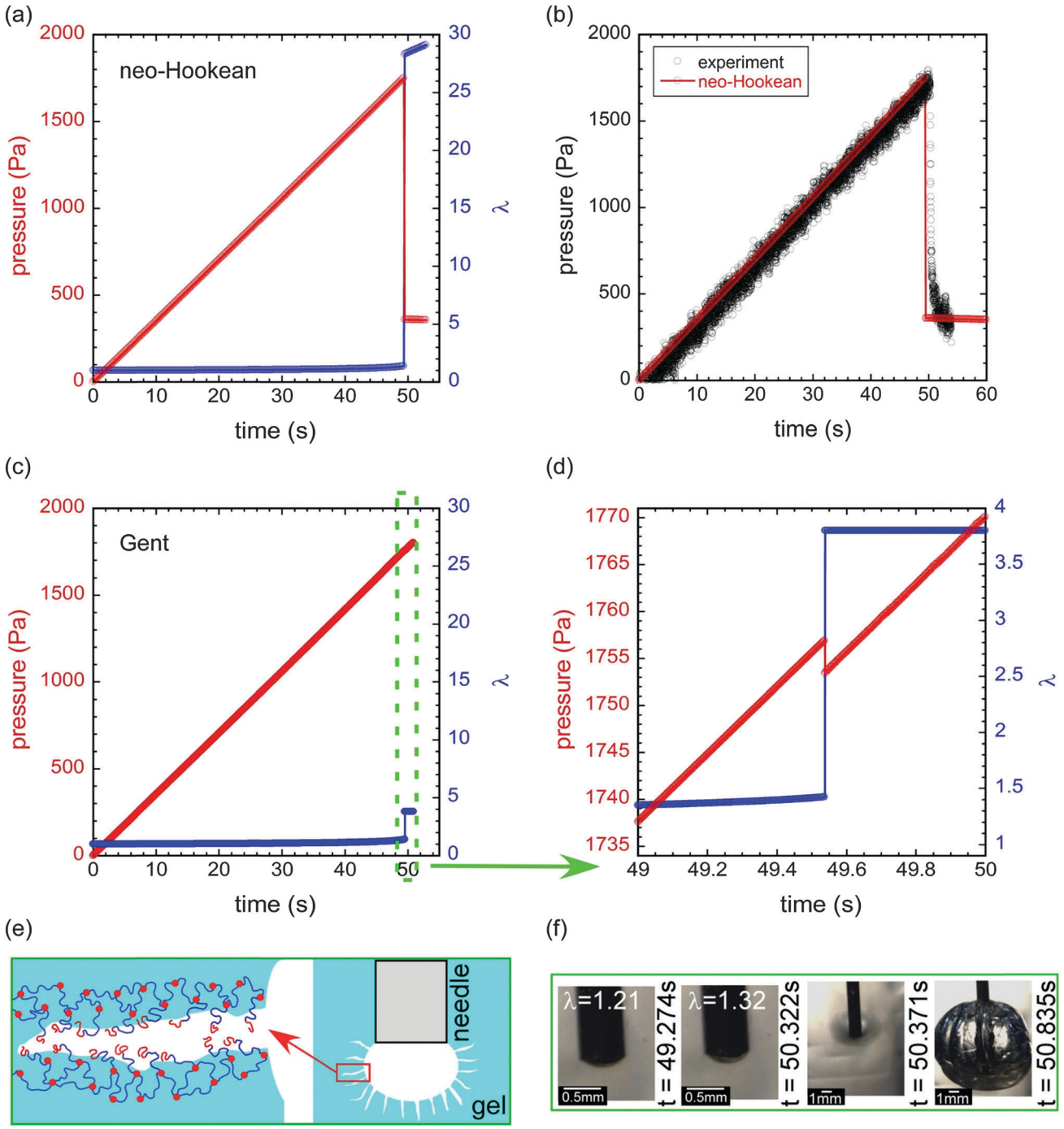

Fig. 7 (a) Predicted pressure and extension ratio as a function of time for a neo-Hookean gel with $\lambda_m \to \infty$; (b) neo-Hookean model prediction compared with the cavitation experimental result; (c) predicted pressure and extension ratio as a function of time for a Gent gel with $\lambda_m = 3.8$; (d) expanded view of (c) at a sudden increase of the expansion ratio; (e) a schematic displaying chain pull out during cavity growth; (f) micrographs before and at critical pressure. Here, for model prediction, $E = 300$ Pa, $r_{in} = 302$ μm, $P_0 = 101325$ Pa, $V_0 = 24$ mL, $\mu = 0.5$ mL min^{-1}, $\Gamma = 0.25$ J m^{-2} are used.

jumps to the vicinity of λ_m, which is equal to 3.8 for this gel (Fig. 6c and d).

The results are summarized in Fig. 7, in which both pressure and extension ratios as a function of time for neo-Hookean and Gent gels are presented. For a neo-Hookean gel (Fig. 7a), as the system is pressurized, an increase of pressure up to a critical point and a sudden drop of pressure beyond that critical point have been predicted. Also, the expansion ratio (λ) increases slowly during the initial compression until a certain jump at the critical point (λ_c = 1.4), caused by the elastic instability, takes place. Since there is no limit of the expansion ratio for neo-Hookean gels ($\lambda_m \rightarrow \infty$), as pressure reaches the instability point, the cavity volume can increase without any bound. Such a rapid increase of cavity volume results in a sudden drop of pressure and cavitation or snap-through expansion is observed. For neo-Hookean gels, the critical pressure can be represented as:[43]

$$P_c = \frac{5}{6}E + \frac{2\Gamma}{r_{in}} \quad (17)$$

This equation is a widely used one.[37,43] Here, the critical pressure for cavitation is related to the elastic modulus of the system and the surface energy. If the surface energy (surface tension) of 2-ethyl-1-hexanol ($\approx$0.0269 J m^{-2})[56] is considered, the predicted Young's modulus (E) value from eqn (17) is much higher than that obtained from the shear-rheological experiments (Fig. S6, ESI†).

For Gent gels, since finite extensibility of chains is considered (λ_m = 3.8, for the present case), the increase of cavity volume is restricted at the instability point. Correspondingly, the pressure decreases slightly at the instability point and then continues to rise (Fig. 7c and d). Both neo-Hookean and Gent models provide the similar prediction up to the critical pressure, but the polymer chain extensibility decides whether a significant decrease in pressure or snap-through expansion is expected. However, for Gent gels, the rise of pressure cannot be unlimited but dictated by the failure or fracture of the gel. Similar to the neo-Hookean gel, cavitation for Gent gels is possible only if λ_m is very large, much larger than 3.8. For the values of E, P_0, V_0, μ, and Γ considered here (Fig. 7), λ_m must be greater than 28.3 to expect cavitation.

Now a large cavity growth was observed for all gels tested here (Fig. 7f). We believe that the cavity growth in our triblock gel is not purely caused by elastic instabilities but a fracture like process is also involved. We hypothesized that during the cavity growth the polymer chains are pulled out of the aggregates (a fracture like process), as schematically represented in Fig. 7e. The critical pressure corresponding to fracture is a function of E, G_c, and r_{in}, where G_c is the critical energy release rate.[24,43] If a material is linear elastic, the critical pressure for fracture scales with $\left(\frac{\pi E G_c}{3 r_{in}}\right)^{\frac{1}{2}}$.[24,43] For non-linear Gent gels, such a functional relationship is not precisely known. Interestingly, if we increase the value of Γ to 0.25 J m^{-2}, eqn (15) can be used to capture the experimental data (Fig. 7b). This signifies that the critical pressure for fracture for the Gent model will likely be linearly dependent on the elastic modulus and G_c, similar to that given by eqn (17). However, the coefficients will be different and it will be appropriate to replace the surface energy term in eqn (17) with a critical energy release rate, G_c, as the process involves fracture. Therefore, $P_c \sim$ constant $\times$ E + function (G_c,r_{in}). Now, there are two unknowns, E and G_c, and one of these must be known to estimate the other. Both E and G_c can be measured experimentally,[27] but the measurement of E using shear rheology is relatively straight-forward. G_c can also be predicted using Lake and Thomas theory.[23] If fracture involves bond-scission, which is very unlikely for our gel, the predicted value of G_c is $\sim$ 0.3 J m^{-2}. For chain pull-out, if we consider the energy associated with pull out one monomer (methylacrylate) unit is $\sim k_B T$, where k_B is the Boltzmann constant, the estimated value of G_c is 0.0005 J m^{-2}, which is unrealistically low. However, the estimated values of G_c from Lake–Thomas theory do not consider viscous dissipation near the crack front, which cannot be ignored in our sample. Our future research will involve implementation of finite-element based modeling to determine the exact mathematical relationship between critical pressure, E, crack length or needle radius, and G_c.

Conclusion

Large-strain deformation behavior of a physically associating, thermally reversible, triblock gel is investigated using shear and cavitation rheology. The Gent model, which considers the finite extension of the midblock, is used to capture the stiffening behavior at large-strain deformation. First (e_1) and third (e_3) Chebyshev coefficients estimated from LAOS analysis are related to the Gent model, *i.e.*, the LAOS parameters have been linked to the gel structure. Cavitation rheology was performed as a function of polymer volume fraction (ϕ), compression rate, and temperature. The pressure response and extension ratio (λ) *vs.* time were modeled using rubber elasticity models such as neo-Hookean and Gent models. Our results show that the neo-Hookean model can capture the experimental data, however, the corresponding surface energy value is high. We hypothesize that the cavitation phenomena observed here include PnBA chain pull out from the PMMA aggregates. Our results provide new understandings on the gel deformation behavior and failure mechanism at large-strain.

Acknowledgements

We gratefully acknowledge the financial support of NSF CAREER Award DMR-1352572 and Mississippi State University start-up funds.

References

1 N. A. Peppas, P. Bures, W. Leobandung and H. Ichikawa, *Eur. J. Pharm. Biopharm.*, 2000, **50**, 27–46.
2 A. S. Hoffman, *Adv. Drug Delivery Rev.*, 2002, **54**, 3–12.

3 R. Langer and J. P. Vacanti, *Science*, 1993, **260**, 920–926.
4 J. L. Drury and D. J. Mooney, *Biomaterials*, 2003, **24**, 4337–4351.
5 P. Calvert, *Adv. Mater.*, 2009, **21**, 743–756.
6 T. Miyata, N. Asami and T. Uragami, *Nature*, 1999, **399**, 766–769.
7 A. E. Way, L. Hsu, K. Shanmuganathan, C. Weder and S. J. Rowan, *ACS Macro Lett.*, 2012, **1**, 1001–1006.
8 Y. Osada, H. Okuzaki and H. Hori, *Nature*, 1992, **355**, 242–244.
9 K. Haraguchi and T. Takehisa, *Adv. Mater.*, 2002, **14**, 1120–1124.
10 K. Haraguchi, K. Murata and T. Takehisa, *Macromolecules*, 2012, **45**, 385–391.
11 Y. M. Kolambkar, K. M. Dupont, J. D. Boerckel, N. Huebsch, D. J. Mooney, D. W. Hutmacher and R. E. Guldberg, *Biomaterials*, 2011, **32**, 65–74.
12 C. He, S. W. Kim and D. S. Lee, *J. Controlled Release*, 2008, **127**, 189–207.
13 W. R. Gombotz and S. Wee, *Adv. Drug Delivery Rev.*, 1998, **31**, 267–285.
14 B. H. Cipriano, S. J. Banik, R. Sharma, D. Rumore, W. Hwang, R. M. Briber and S. R. Raghavan, *Macromolecules*, 2014, **47**, 4445–4452.
15 B. Jeong and A. Gutowska, *Trends Biotechnol.*, 2002, **20**, 305–311.
16 B. A. Trimmer and H. Lin, *Integr. Comp. Biol.*, 2014, icu076.
17 M. A. Haque, T. Kurokawa and J. P. Gong, *Polymer*, 2012, **53**, 1805–1822.
18 C. Storm, J. J. Pastore, F. C. MacKintosh, T. C. Lubensky and P. A. Janmey, *Nature*, 2005, **435**, 191–194.
19 J. Zhang, C. R. Daubert and E. Allen Foegeding, *J. Food Eng.*, 2007, **80**, 157–165.
20 K. A. Erk, K. J. Henderson and K. R. Shull, *Biomacromolecules*, 2010, **11**, 1358–1363.
21 M. Rubinstein and S. Panyukov, *Macromolecules*, 2002, **35**, 6670–6686.
22 M. Rubinstein and R. H. Colby, *Polymer Physics*, Oxford University Press, 2003.
23 G. J. Lake and A. G. Thomas, *Proc. R. Soc. London, Ser. A*, 1967, **300**, 108–119.
24 Y. Y. Lin and C. Y. Hui, *Int. J. Fract.*, 2004, **126**, 205–221.
25 T. Baumberger, C. Caroli and D. Martina, *Nat. Mater.*, 2006, **5**, 552–555.
26 Y. Tanaka, R. Kuwabara, Y.-H. Na, T. Kurokawa, J. P. Gong and Y. Osada, *J. Phys. Chem. B*, 2005, **109**, 11559–11562.
27 M. E. Seitz, D. Martina, T. Baumberger, V. R. Krishnan, C.-Y. Hui and K. R. Shull, *Soft Matter*, 2009, **5**, 447–456.
28 K. A. Erk and K. R. Shull, *Macromolecules*, 2011, **44**, 932–939.
29 Y. Akagi, H. Sakurai, J. P. Gong, U. Chung and T. Sakai, *J. Chem. Phys.*, 2013, **139**, 144905.
30 G. Miquelard-Garnier, D. Hourdet and C. Creton, *Polymer*, 2009, **50**, 481–490.
31 W.-C. Lin, W. Fan, A. Marcellan, D. Hourdet and C. Creton, *Macromolecules*, 2010, **43**, 2554–2563.
32 K. Hyun, M. Wilhelm, C. O. Klein, K. S. Cho, J. G. Nam, K. H. Ahn, S. J. Lee, R. H. Ewoldt and G. H. McKinley, *Prog. Polym. Sci.*, 2011, **36**, 1697–1753.
33 E. S. Vasquez, J. Bowser, C. Swiderski, K. B. Walters and S. Kundu, *RSC Adv.*, 2014, **4**, 34780–34783.
34 M. Wilhelm, *Macromol. Mater. Eng.*, 2002, **287**, 83–105.
35 R. H. Ewoldt, A. E. Hosoi and G. H. McKinley, *J. Rheol.*, 2008, **52**, 1427–1458.
36 K. S. Cho, K. Hyun, K. H. Ahn and S. J. Lee, *J. Rheol.*, 2005, **49**, 747–758.
37 J. A. Zimberlin, N. Sanabria-DeLong, G. N. Tew and A. J. Crosby, *Soft Matter*, 2007, **3**, 763–767.
38 J. A. Zimberlin, J. J. McManus and A. J. Crosby, *Soft Matter*, 2010, **6**, 3632–3635.
39 P. Fei, S. J. Wood, Y. Chen and K. A. Cavicchi, *Langmuir*, 2014, **31**, 492–498.
40 L. Pavlovsky, M. Ganesan, J. G. Younger and M. J. Solomon, *Appl. Phys. Lett.*, 2014, **105**, 114105.
41 M. L. Williams and R. A. Schapery, *Int. J. Fract. Mech.*, 1965, **1**, 64–72.
42 A. N. Gent, *Int. J. Non Linear Mech.*, 2005, **40**, 165–175.
43 S. Kundu and A. J. Crosby, *Soft Matter*, 2009, **5**, 3963–3968.
44 J. Zhu, T. Li, S. Cai and Z. Suo, *J. Adhes.*, 2011, **87**, 466–481.
45 S. B. Hutchens and A. J. Crosby, *Soft Matter*, 2014, **10**, 3679–3684.
46 A. Delbos, J. Cui, S. Fakhouri and A. J. Crosby, *Soft Matter*, 2012, **8**, 8204–8208.
47 D. L. Henann and K. Bertoldi, *Soft Matter*, 2014, **10**, 709–717.
48 T. Goudarzi and O. Lopez-Pamies, *J. Appl. Mech.*, 2013, **80**, 050906.
49 P. L. Drzal and K. R. Shull, *Macromolecules*, 2003, **36**, 2000–2008.
50 A. Nakagawa, G. T. Manley, A. D. Gean, K. Ohtani, R. Armonda, A. Tsukamoto, H. Yamamoto, K. Takayama and T. Tominaga, *J. Neurotrauma*, 2011, **28**, 1101–1119.
51 M. E. Seitz, W. R. Burghardt, K. T. Faber and K. R. Shull, *Macromolecules*, 2007, **40**, 1218–1226.
52 K. A. Erk and J. F. Douglas, *MRS Online Proc. Libr.*, 2012, **1418**, DOI: 10.1557/opl.2012.335.
53 S. R. Raghavan and J. F. Douglas, *Soft Matter*, 2012, **8**, 8539–8546.
54 L. R. G. Treloar, *The Physics of Rubber Elasticity*, Oxford University Press, 1975.
55 A. N. Gent, *Rubber Chem. Technol.*, 1999, **72**, 263–268.
56 N. P. Cheremisinoff, *Industrial Solvents Handbook, Revised and Expanded*, CRC Press, 2003.